Pergamon

PII:S0899-5362(00)00019-1

Journal of African Earth Sciences, Vol. 30, No. 2, pp. 267–282, 2000

0899-5362/00 $- see front matter

A genetic model for a mesothermal Au deposit: evidence from fluid inclusions and stable isotopic studies at El Sid Gold Mine, Eastern Desert, Egypt

HASSAN Z. HARRAZ*
Department of Geology, Faculty of Science, Tanta University, Tanta, Egypt

ABSTRACT—The El Sid Au mineralisation in the Fawakhir area, Eastern Desert, Egypt, is comprised of hydrothermal quartz veins cutting a Neoproterozoic granitoid pluton. The mineralisation is divided into Au-bearing, transitional and late carbonate vug stages. Pyrite-arsenopyrite and streaky pyrite-sphalerite-galena assemblages characterise the early and late episodes of the Au-bearing stage, respectively. These sulphide minerals sometimes contain Au as inclusions.

Fluid inclusions from the Au-bearing stage are H_2O-CO_2-rich fluids (*ca* 29–62 mole% CO_2 and density, *ca* 0.51–0.66 g cm^{-3}) with moderate to high salinities (*ca* 12–19 wt% NaCl equiv.). The trapping temperature of the ore occurred between 280 and 350°C, at pressures between 120–170 MPa (~800–1800 m depth). However, fluid inclusions from the pyrite-arsenopyrite assemblage reflect lower homogenisation temperature measurements (T_h) (265–295°C) than those in the streaky pyrite-sphalerite-galena assemblage (330–365°C). The minerals of the transitional and late carbonate vug stages (quartz and calcite) were formed between 180 and 265°C.

Oxygen and H isotope data of fluid inclusions hosted in the quartz and calcite from the Au-bearing stage indicate a rather wide range of calculated $\delta^{18}O_{H_2O}$ and δD_{H_2O} (i.e. +3.2 to +7.8‰ and -75 to -32‰, respectively). The data for the streaky pyrite-sphalerite-galena assemblage exhibit higher $\delta^{18}O_{H_2O}$ values (+5.3 to +6.8‰) and lower δD_{H_2O} (-75 to -48‰) relative to that of the pyrite-arsenopyrite assemblage. Calculated isotopic temperatures of quartz-calcite fractionation range from 282 to 353°C and are consistent with the trapping temperatures (280–350°C).

The fluid inclusion and stable isotope data imply that Au at the El Sid Gold Mine has been transported as a bisulphide complex. The high salinity and inferred occurrence of CH_4 in some fluid inclusions collected from the graphite-rich zone along a serpentinite-granitoid contact suggest that the mineralising solutions gained their metal contents through circulation in the fractured zones and incorporation with a geothermal convective system by wall rock interaction. Deposition of Au sulphides has taken place at shallow crustal levels (~800–1800 m) as a result of meteoric/magmatic-metamorphic water exchange with wall rocks through H_2O-CO_2 immiscibility during fluid pressure drop and decreasing ligand activity.

RÉSUMÉ—Le gisement d'Au d'El Sid dans la région de Fawakhir, Désert Oriental, comprend des veines de quartz hydrothermal recoupant un pluton granitique néoprotérozoïque. La minéralisation s'est formée au cours de trois stades: à Au, transitionnel et à géodes de carbonates tardifs. Les assemblages à pyrite-arsénopyrite et à pyrite-sphalérite-galène en bandes caractérisent, respectivement, les épisodes précoces et tardifs du stade à or. Les sulfures contiennent parfois de l'Au en inclusions.

Les inclusions fluides du stade à Au sont riches en H_2O et CO_2 (de 29 à 62 moles% de CO_2 et densité de 0.51 à 0.66 g cm^{-3}) avec une salinité modérée à forte (12–19 poids% en équivalent NaCl). La température de capture du minerai se situe entre 280 et 350°C pour une pression entre

*hharraz@dec1.tanta.eun.eg

120 et 170 MPa (soit une profondeur de 800 à 1800 m). Cependant, les températures d'homogénéisation (T_h) des inclusions fluides de l'assemblage à pyrite-arsénopyrite sont plus basses (265–295°C) que celles de l'assemblage à pyrite-sphalérite-galène en bandes (330–365°C). Les minéraux (quartz et calcite) des stades transitionnel et à géodes de carbonates tardifs se sont formés entre 180 et 265°C.
Les valeurs isotopiques de l'O et de l'H des inclusions fluides du quartz et de la calcite du stade à Au montrent une très grande variation des valeurs calculées de $\delta^{18}O_{H_2O}$ et δD_{H_2O} (soit +3.2 à +7.8‰ et -75 à -32‰, respectivement). L'assemblage à pyrite-sphalérite-galène en bandes présente des valeurs de $\delta^{18}O_{H_2O}$ plus fortes (+5.3 à +6.8‰) et de δD_{H_2O} plus faibles (-75 à -48‰) que l'assemblage à pyrite-arsénopyrite. Les températures calculées du fractionnement isotopique quartz-calcite varient de 282 à 353°C, en accord avec les températures de capture (280–350°C). Les données sur les inclusions fluides et les isotopes stables impliquent que l'Au de la mine d'El sid a été transporté sous forme de complexes bisulfurés. La forte salinité et la présence supposée de CH_4 dans quelques inclusions fluides prises dans la zone à graphite le long d'un contact entre serpentinite et granitoïde suggèrent que les solutions minéralisatrices ont acquis leurs teneurs en métaux en circulant dans les zones de fractures et en réagissant avec les roches encaissantes à l'intérieur d'un système géothermique convectif. Le dépôt de sulfures d'Au a pris place à des niveaux crustaux superficiels (800–1800 m) à la suite d'échanges entre les eaux météoriques/magmatiques-métamorphiques et les roches encaissantes, par immiscibilité dans le système H_2O-CO_2 par chute de la pression de fluides et baisse de l'activité des ligands.

(Received 24/8/98: revised version received 27/11/99: accepted 17/11/99)

INTRODUCTION

Gold mineralisation is widely distributed in the Arabo-Nubian Shield and its genesis is discussed in several works (Garson and Shalaby, 1976; El-Gaby *et al.*, 1988; Pohl, 1988). Most of these Au deposits are hosted by intrusives, volcanics, ophiolitic rocks and post-orogenic granites (Pohl, *op. cit.*). The majority of these deposits occur as Au-bearing quartz veins of polymetallic character, closely associated with granitoids (El-Bouseily *et al.*, 1985; Harraz and El-Dahhar, 1993) and largely controlled by two prominent fracture systems which dominated the Eastern Desert (El-Gaby *et al.*, 1988; Sabet and Bondonosov, 1984; Harraz and Ashmawy, 1994). The occurrence in the El Sid-Fawakhir area (Fig. 1A) is an example of such a deposit.

The El Sid-Fawakhir area is located 93 km west of the Red Sea Coast, along the Qift-Quseir Highway in the Eastern Desert of Egypt (Fig. 1A). It is one of several Au mines in the Eastern Desert of Egypt which has been extensively worked since Pharaonic and Roman times. Mining activity ceased in 1958. The El Sid Gold Mine (26°00'17"N, 33°35'42"E) is considered to be the largest mesothermal vein type Au occurrence in the Eastern Desert of Egypt (Sabet and Bondonosov, 1984; Hussein, 1990) where the mineralised quartz veins are hosted mainly in granitoid rocks. It accounts for ~45% of the Au production in Egypt with a total production of 2653 kg of Au (20.6–27.9 g t^{-1} Au) in the period 1944–1958 (Hussein, 1990). The ore was exploited mainly from quartz veins to ~160 m in depth. However, it is believed that the potential of the deposit has not been exhausted yet. For much of the mine's history, Au was exploited only from major quartz veins and some veinlets cutting the hanging and footwalls of the main ore bodies. About 178 quartz, quartz-calcite veins, veinlets and zones of silicification are known in the El Sid Gold Mine field. The majority of them had been worked out in ancient times to a depth of ~30 m. Gold grades in lump samples, mainly taken from pillars, range from traces to 40.8 g t^{-1} with an average 8.9 g t^{-1} of Au. Harraz (1985) evaluated three zones (~60–150 m thick) in the southern, central and northern blocks of the mine with Au contents reaching as much as 3 g t^{-1}.

This paper focuses on the application of fluid inclusion and stable isotope analysis to the Au-bearing quartz veins at El Sid Gold Mine to determine the composition and nature of the parent mineralising fluids. A genetic model for mesothermal Au deposit is further discussed.

GEOLOGICAL SETTING

The El Sid-Fawakhir area (Fig. 1A) comprises a distinct association of Precambrian rocks including serpentinites, metagabbro-diorite complex, metavolcanic-metasediments and the Fawakhir granitoid pluton (Fig. 1A). The Fawakhir granitoid pluton (~25 km^2) belongs

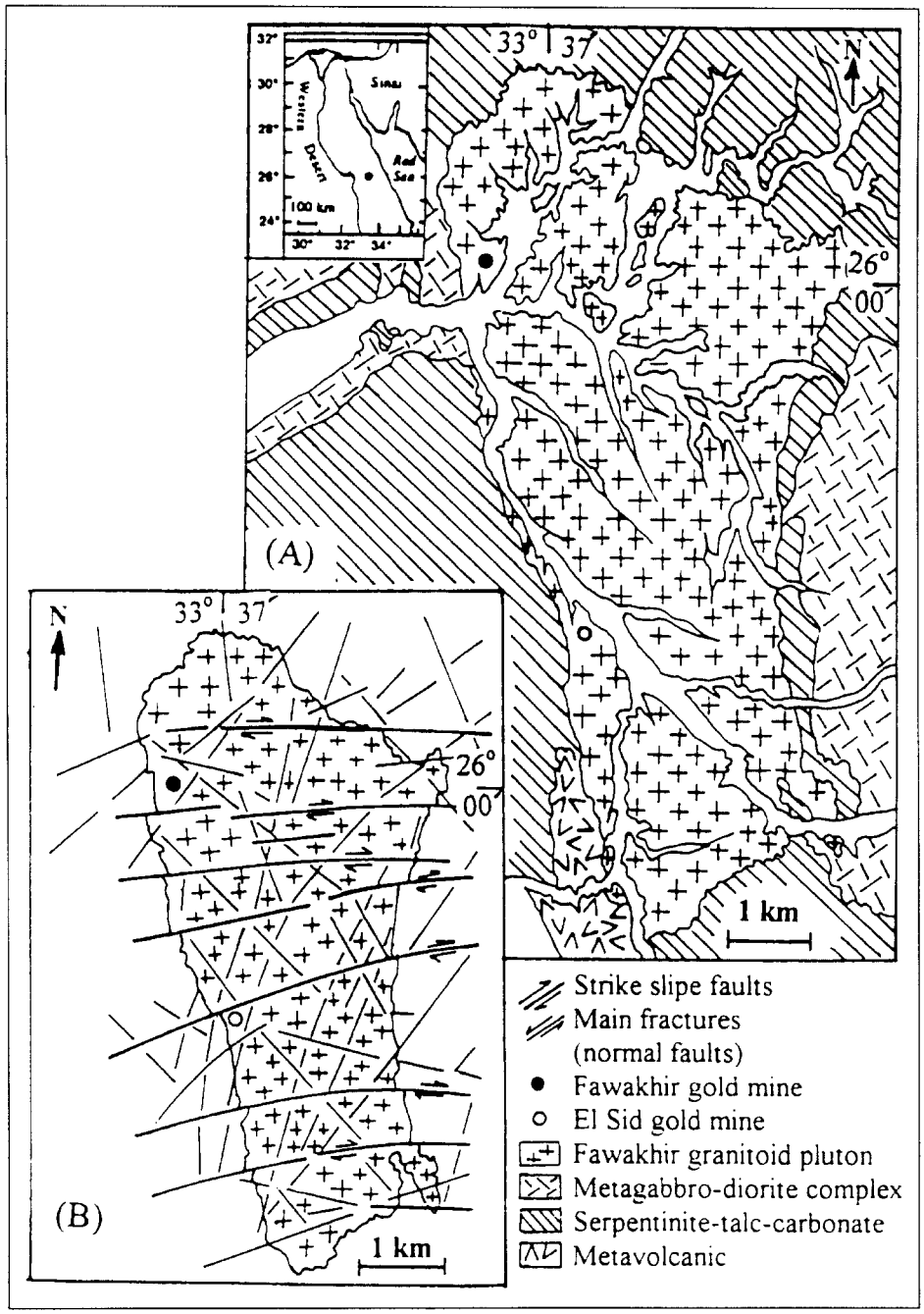

Figure 1. *(A) Location and simplified geological map of the El Sid-Fawakhir area. (B) Detailed structural map of the El Sid-Fawakhir area (after Harraz and Ashmawy, 1994).*

to the early phase of the Pan-African granites of *ca* 585–590 Ma (Meneisy and Lenz, 1982), which were mainly intruded into serpentinites. The serpentinite rocks form a large envelope around the Fawakhir granitoid pluton and are regarded as a member of an ophiolitic sequence developed in a subduction zone (El-Mezayen, 1983). The Fawakhir Pluton is inhomogeneous, incorporating a variety of colours including gray, pale pink and red. Compositionally, it ranges from granodiorite and hornblende granite to differentiated pale pink biotite granite. The granodiorite and hornblende granites are rich in mafic xenoliths (restite types), which predominate along the west margin of the pluton, particularly near the El Sid Gold Mine. The central part of the pluton is a differentiated pink biotite granite. Numerous acidic to intermediate dykes and quartz veins dissect the Fawakhir granitoid in a general north-northeast direction and occasionally extend into the surrounding serpentinites.

The regional fault pattern in the study area is dominated by three major trends that follow east-northeast, north-northeast, and north-northwest to

northwest directions, while a west-northwest fault trend is less significant (Fig. 1B). The east-northeast trending faults are mainly strike-slip of right-lateral type, while the other trends are mostly of normal type and steeply inclined to near vertical. The east-northeast strike-slip faults are younger than the other trends on the basis of the last activity (Harraz and Ashmawy, 1994). The mineralised quartz veins at the El Sid Gold Mine are closely associated with the intersections of east-northeast strike-slip faults with the north-northeast and north-northwest faults (Fig. 1B).

Main lode

Mineralisation occurs within fissure-filling quartz veins exposed at the northern and western contacts of the Fawakhir granitoid pluton with the serpentinites and metagabbro complexes (Fig. 1). The main quartz vein lodes in both sites are conformable to the east-northeast–west-southwest fracture trend. The western occurrence (the El Sid Gold Mine) is the largest one. The auriferous quartz veins crop out at the contact between granitic and serpentinite rocks, but occasionally extend into the metagabbro complexes through a thick zone (~15 m) of graphite schist (Fig. 2). Other quartz veins extend throughout the different underground levels and invade a shear zone which is filled by pockets of quartz and mixture of graphite, carbonate and chlorite materials that crosses the granodiorite-metagabbro complex contact. The veins are formed mainly of massive milky to gray quartz with or without carbonate (calcite, ankerite and siderite), chlorite and sulphide minerals.

The main lode has been exploited for ~280 m along its strike and via three inclined shafts, to 160 m down dip. The mineralised quartz veins have a general east-northeast–west-southwest direction (with dips 42°SE) and north-northeast–south-southwest (with dips 65°SE). The dip of these quartz veins change

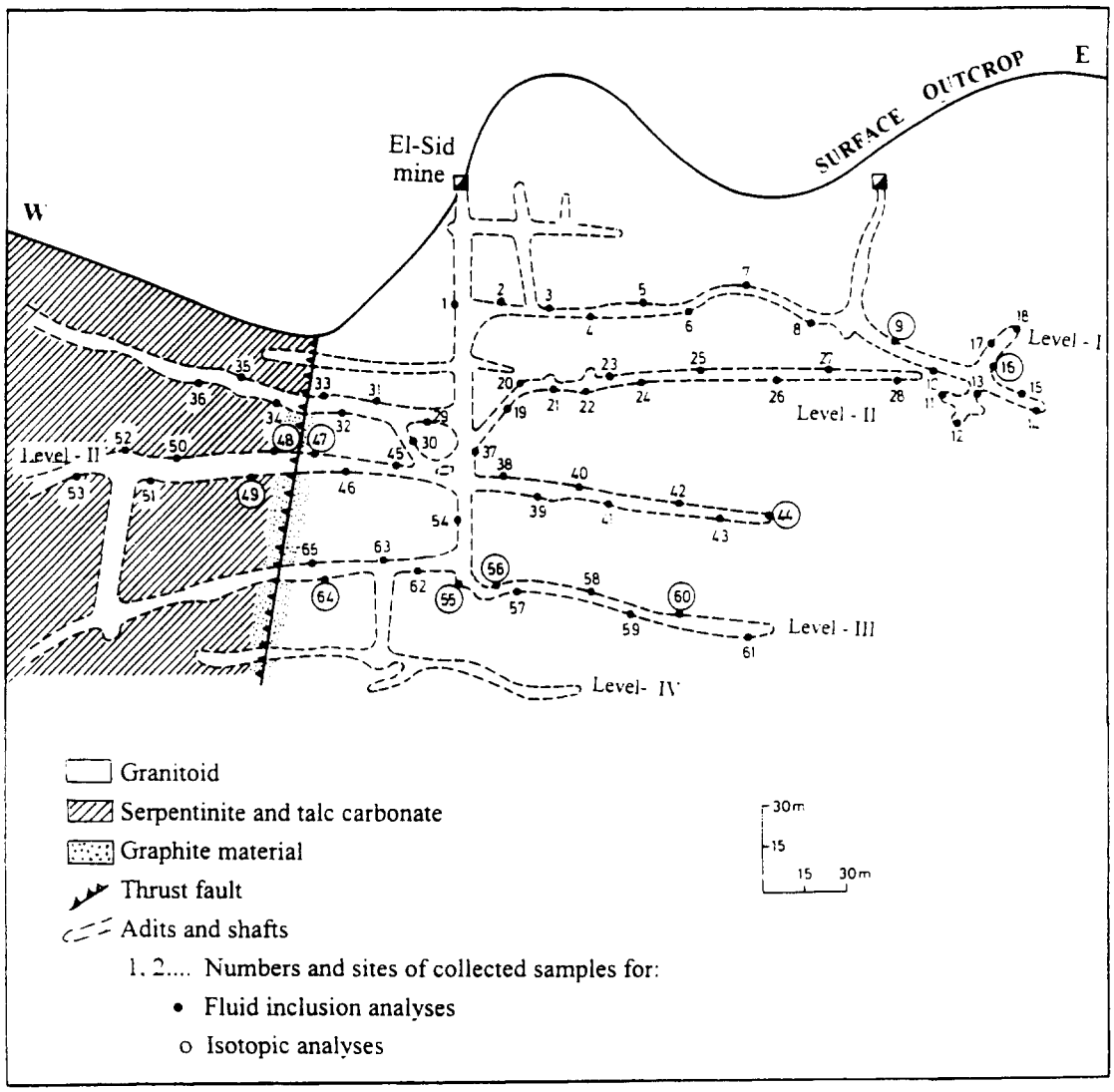

Figure 2. Longitudinal cross-section in the El Sid Gold Mine showing the different levels of the mine workings and locations of the analysed samples. The traced levels of mining activity are taken from the Au mine authorities.

from 64°S to 70°S with depth. They vary in width from a few centimetres to 1.5 m. Large veins extend discontinuously up to 1100 m along strike and ~455 m down dip (Hussein, 1990), largely controlled by sublatitudinal and east-northeast fracture systems. They usually pinch, swell, bifurcate into smaller veins, veinlets and stringers (off-shoots), and join other veins, giving rise to a network pattern (~100 m wide). These veins are typically multiphase, exhibit an *enechelon*-like structure, and contain wall rock fragments.

The Au-bearing quartz veins contain appreciable amounts of Fe, As, Pb, Zn, Cu and Ag sulphides. The average Au content of the El Sid mineralisation varies considerably from 1.5 to 22.6 g t^{-1} and it may reach as much as 29.7 g t^{-1} in quartz-calcite veins. Generally, the Au content decreases with depth. Silver is also present to as much as 22.9 g t^{-1} (Hussein, 1990). The highest Au contents are determined in the pyrite-rich zones, which may be ~1 m thick, depending on the thickness of the veins. The wall rocks in close vicinity of the mineralised quartz vein suffered, in places, intensive hydrothermal silicification, chloritisation and pyritisation (El-Dahhar, 1995). Barren quartz veins trend north-northwest–south-southeast and dip 54° to the southwest.

ORE MICROSCOPY AND MINERAL PARAGENESIS

The principal sulphide minerals in the El Sid Gold Mine are mostly pyrite, arsenopyrite, sphalerite, galena and minor pyrrhotite and chalcopyrite, associated with quartz and/or carbonate gangue. They occur randomly as fine- to medium-grained interlocking aggregates and as disseminations in the quartz veins. The abundance of these sulphides tends to increase with depth.

A general paragenetic sequence (Fig. 3) of the sulphide minerals is given by El- Bouseily *et al.* (1985). They recognised two successive stages on the basis of textural relationship: an early stage dominated by pyrite-arsenopyrite and a late one represented by sphalerite-galena. However, further microscopic inspection of both stages revealed the presence of:

i) Pyrrhotite and magnetite together with minor amounts of sphalerite and galena in the former (pyrite

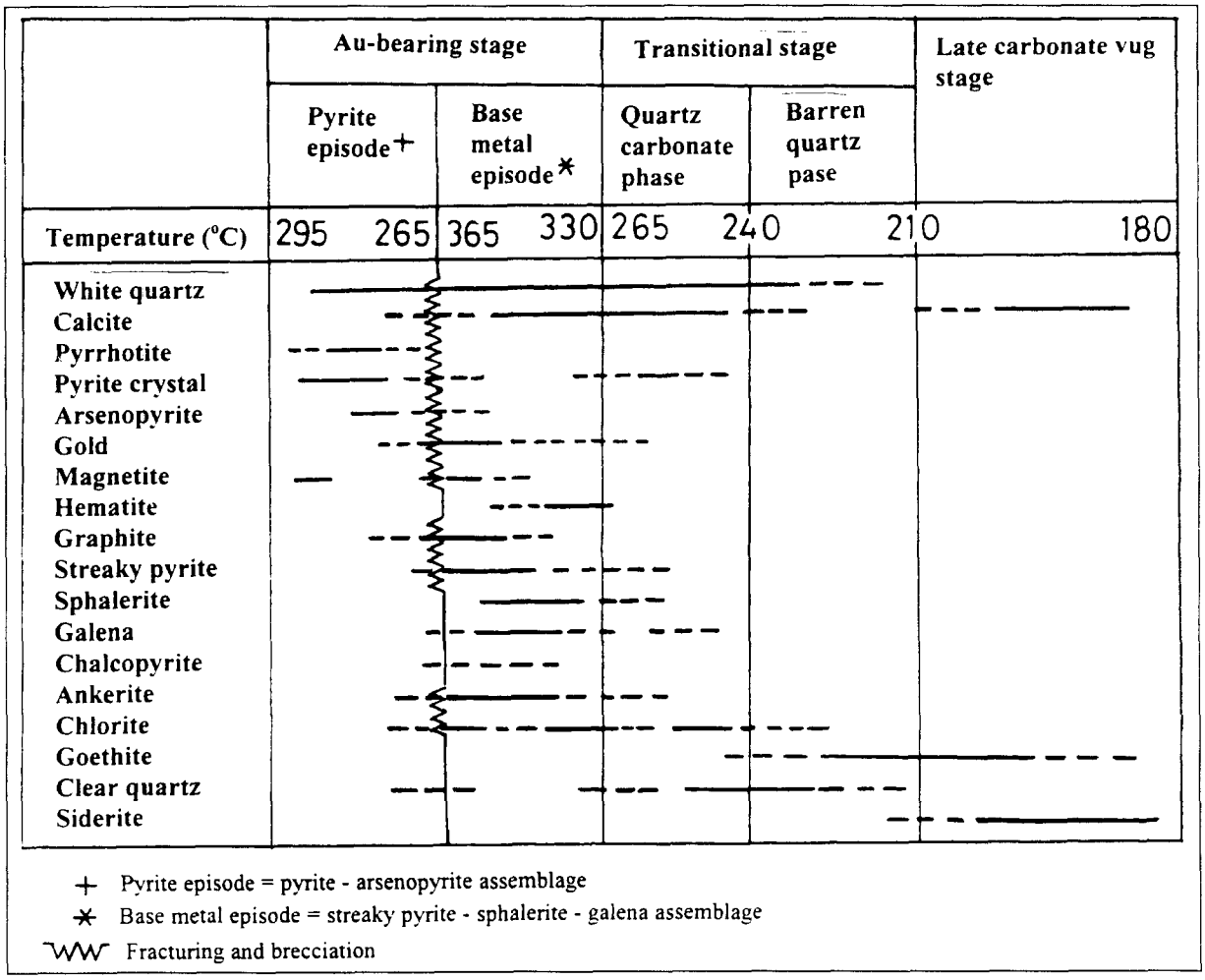

Figure 3. *Paragenetic sequence of minerals from the El Sid Gold Mine area. The temperature scale is based on fluid inclusion analysis.*

stage) and streaky to very fine-grained pyrite and ankerite in the latter (base metal stage). For simplicity the two stages are assigned as Au-bearing stages in this study.

ii) Two other stages could be recognised:

a) A transitional stage marked by either a scarce amount of very fine-grained sphalerite, galena and pyrite in quartz and carbonate materials (quartz-carbonate phase); and sulphide-free quartz veins with selvedge of fine-grained siderite and goethite (barren quartz phase).

b) A late carbonate vug stage composed, almost entirely, of calcite with minor siderite. Calcite commonly occurs along fractures and in vugs forming drusy aggregates.

Gold is present as fine disseminated specks in quartz gangue and as infiltrations along microfractures in coarse-grained pyrite and arsenopyrite and as blebs (<0.1 μm) in the sphalerite. This may indicate that most of the Au was deposited at the beginning of the streaky pyrite-sphalerite-galena association or at least coincident with sphalerite crystallisation.

Patterns of hydrothermal alteration in the area studied are simple silicification and sericitisation of granitic rocks, while chloritisation and carbonatisation are dominant in the serpentinites (El-Dahhar, 1995). Minor graphitic material is also developed in shear zones and fractures close to the contact of the granitoids and serpentinite, mostly encountered at level II (Fig. 2). Wall rocks surrounding the Au-bearing quartz veins are characterised by abundant silicification-carbonatisation and rare chloritisation alterations.

SAMPLE SELECTION AND ANALYTICAL TECHNIQUES

For the purpose of this study, four types of materials were selected:

i) white quartz intimately associated with Au-bearing sulphides;

ii) clear quartz and calcite from the alteration zone;

iii) barren quartz veins; and

iv) calcite crystals filling vugs.

Fluid inclusions were examined in thin (<0.30 mm thick) doubly polished slices. Microthermometric measurements were performed using the Linkam THM-600 programmed heating-freezing stage (Shepherd, 1981), attached to an Olympus (BH-2) microscope, connected with a television camera and screen (housed at the Mineralogical Museum, Toyen-Oslo University, Norway). The measurements were conducted only on primary and pseudosecondary fluid inclusions. The warming rate was maintained at about 1°C min.$^{-1}$. The cooling rate is difficult to control but it generally falls between 5 and 15°C min.$^{-1}$. Super-cooling was necessary for the freezing of both CO_2-hydrate and ice. Homogenisation temperatures were determined by observing the temperature at which the boundary between liquid CO_2 and H_2O disappears. A heating rate of 5°C min.$^{-1}$ was used during the initial stages of each heating run and reduced to 2°C min.$^{-1}$ close to the homogenisation temperature. Decrepitation was not observed before the final homogenisation temperature. Pressure corrections, which should be minimal in a 'boiling' system, were not applied. Replicate measurements of homogenisation and melting temperatures of standard H_2O- and CO_2-rich fluid inclusions in quartz from Calanda, Ticine and the Swiss-Alps and organic compounds with different known melting points were used (Table 1).

Salinities were calculated using the final melting temperatures of CO_2-clathrate (Collins, 1979) and ice (Roedder, 1963) and expressed as NaCl wt% equiv. The homogenisation temperature of the CO_2-rich phase in inclusions ($T_{h_{CO_2}}$ L-V), together with volume data on phase ratios (calculated from relative areas)

Table 1. Types of thermometric measurement made on inclusions and their estimated reproducibility

Measurement	Abbreviation	Reproducibility (°C)
Final melting of ice	$T_{m_{ice}}$	±0.3
Final melting of clathrate	T_{Clath}	±0.3
Initial melting of CO_2 phase	$T_{m_{CO_2}}$	±0.3
Homogenisation within CO_2 phase	$T_{h_{CO_2}}$ L-V	±1.0
Total homogenisation of inclusion contents	T_h	±1.0

are used in calculating the molar ratios of CO_2 and H_2O and the fluid density.

Isotopic analyses of O and H were performed on separated calcite and quartz from nine country rock samples representing the three paragenetic stages and depth variation in the El Sid Gold Mine. The quartz and calcite used for isotopic analyses were separated from the 125–250 μm fraction using Na-Polytungstate solution and Franz Isodynamic Separation. The purity reached for the studied phases is in excess of 95%.

The O and H isotopes of the quartz and calcite minerals were performed at the stable isotope laboratory of the University of Bergen-Norway, with a Finnigan Mat Mass Spectrometer, following the procedure outlined by Rye and Sawkins (1974). Isotopic data are reported in standard δ notation relative to SMOW (Craig, 1961) for O and H. The standard error for each analysis is approximately ±0.1‰ for O and ±2‰ for H.

FLUID INCLUSION STUDY

Eighty-four fluid inclusions were examined in quartz and calcite materials from all stages of mineralisation in the El Sid Gold Mine. Locations of the selected samples are shown in Fig. 2.

Two major types of fluid inclusions are recognised, namely liquid-rich and vapour-rich inclusions. Liquid-rich inclusions constitute 10–40% of the total volume of all detected inclusions at room temperature. The vapour-rich inclusions consist of a large vapour bubble (>70 vol.%) at room temperature and a minor liquid phase. Generally, the fluid inclusions range in size from 10 to 20 μm. Most of these inclusions are arranged along lines of crystal growth. There is no evidence of deformation and thus they are considered as primary and/or pseudosecondary fluids according to the criteria defined by Roedder (1967). Collectively, the two types have rounded shapes and exhibit a relatively wide range of liquid/vapour volume ratios indicating heterogeneity of the trapped liquid-vapour mixtures. Data of the inspected fluid inclusions are summarised in Table 2 and plotted in Figs 4 and 5.

Apparently, the fluid inclusion data reveal wide and different ranges between the Au-bearing, transitional and late carbonate vug stages. Plotting of salinity (wt% equiv.) versus T_h (Fig. 4) also allows discrimination between the three paragenetic stages of the studied mineralisation. The Au-bearing stage is characterised by fluid inclusions of high salinity (12–19 wt% equiv.) and T_h (265–365°C). Although, the pyrite and base metal episodes have the same salinity range, the latter reflects higher T_h than the former. The transitional stage is characterised by moderate salinity (7–12 wt% equiv.) and T_h (210–265°C). The quartz-carbonate and barren quartz phases have a similar salinity range, nevertheless the former reflects higher T_h than the latter. The late carbonate vug stage is characterised by low salinity (4–8 wt% equiv.) and T_h (180–210°C). These may reflect a continuum of three hydrothermal episodes during the formation of the quartz and calcite in the El Sid Gold Mine rather than one single event (Roedder, 1984; Nesbitt, 1993), which will be discussed below.

The Au-bearing stage

The Au-bearing stage is characterised by CO_2-rich inclusions, probably with methane (CH_4) (Burruss, 1981) as indicated by *a* $T_{m_{CO_2}}$ (clustered at around -56.3°C; Fig. 5A) lower than pure CO_2 (-56°C). A common feature for Au deposits, in which CH_4 is inferred in fluid inclusions, is the presence of 'graphitic material' (Ho *et al.*, 1985). The occurrence of graphitic material at the El Sid Gold Mine may be attributed to the serpentinite alteration by fluid wall rock reactions. This is in agreement with the conditions encountered in the studied samples from level II west at El Sid Gold Mine (nos 48–53; Fig. 2). Consequently, the presence of CH_4 indicates that reduction may have played a significant role in Au deposition (Bottrell *et al.*, 1988; Naden and Shepherd, 1989) since CH_4 was not a component of the original fluids.

The homogenisation of CO_2-rich liquid-vapour phases (always to a vapour) within the Au-bearing stage (Fig. 5B) was measured in the absence of ice and clathrate compounds. Fluid inclusions from the pyrite episode show a wide range of $T_{h_{CO_2}}$ L-V (+28.0 and +31.5°C), while those in the base metal episode range between +22.0 and +26.5°C (Fig. 5B). Estimated CO_2 densities for inclusions in the Au-bearing stage range from 0.51 to 0.77 g cm^{-3}. The base metal episode is charac-terised by a slightly higher CO_2 density (0.60–0.77 g cm^{-3}) than the pyrite episode (0.51–0.66 g cm^{-3}). These fluid inclusions contain pure CO_2-H_2O where CO_2 forms 29.2–56.9 mole% in the pyrite episode and 29.0–62.5 mole% in the base metal episode.

The majority of T_{Clath} and $T_{m_{ice}}$ data of the fluid inclusions from the pyrite episode fall around +1.0 and -10.3°C, respectively, while in the base metal episode they cluster near -1.5 and -13.3°C, respectively (Table 2 and Fig. 5C, D). The depression of clathrate (in the presence of CO_2 liquid and vapour, and H_2O liquid) amounts to a salinity 14.5 wt% equiv. in the pyrite episode and 17.5 wt% equiv. in the base metal episode (Table 2 and Fig. 4). Depression of the melting temperature for clathrate compounds for relatively pure H_2O-CO_2-NaCl fluid ($T_{m_{CO_2}}$ -56.3°C) indicates the presence of X_{NaCl} ranging from 3.3 to 6.3 mol.% in the pyrite episode and 3.1 to 6.5 mol.% in the base metal episode (Table 2).

Table 2. Description of fluid inclusions from El Sid Gold Mine and the nature of the trapped fluids

		Au-bearing stage		Transitional stage		Late-carbonate vug stage
		Pyrite episode	**Base metal episode**	**Quartz-carbonate phase**	**Barren quartz phase**	
Sample type		Milky, massive quartz with calcite with pyrite and arsenopyrite	Milky quartz pods in massive quartz veins with sulfide minerals	Least deformed thin, milky and clear quartz and calcite	Thin, massive barren quartz	Clear calcite veinlets with quartz crystals in vugs siderites
Fluid inclusion: Type Size		10 µm b(i) and b/d	25 µm c(ii) and a/c	50 µm usually 20 µm b(i) and b/d	30 µm e(i) and d/e	20 µm a(i) and a(ii)
	$T_{h_{CO_2}}$ L-V (°C)	28 to 31.5	22.0 to 26.5	18.5 to 21.5		12.5 to 15.5
	$T_{m_{ice}}$ (°C)	-14.5 to -8.0	-14.5 to -9.5	-4.0 to -6.5	-8.5 to -5.5	
	T_{Clath} (°C)	-2.0 to +3.5	-3.0 to +1.5	+4.2 to +6.5		+4.5 to +7.5
	$T_{m_{CO_2}}$ (°C)	-58.3 to -56.0	-57.7 to -56.0	-57.5 to -56.0		-57.5 to -56.0
	T_h (°C)	265 to 295	330 to 365	246 to 265	210 to 235	180 to 210
	Wt% NaCl equiv.	12 to 18	12 to 19	7 to 11	7 to 12	4 to 8
	X_{NaCl}	3.26 to 6.27	3.08 to 6.48	2.22 to 3.58	2.37 to 4.40	
	X_{CO_2}	29.24 to 56.92	28.98 to 62.53	34.08 to 62.85		28.78 to 51.60
	d_{CO_2}	0.51 to 0.66	0.60 to 0.77	0.72 to 0.79		0.82 to 0.87
	d_{H_2O}	1.07 to 1.12	1.06 to 1.13	1.05 to 1.07	1.05 to 1.11	
	d_{total}	0.64 to 0.82	0.72 to 0.92	0.77 to 0.88	0.13 to 0.21	0.89 to 0.93
Comments and significance of results		Problems with small inclusions with regard to $T_{m_{ice}}$	Represents the Au bearing quartz veins El Sid Au deposit	Considered as typical alteration assemblages associated with the Au bearing quartz vein at El Sid Au deposit	Typical El Sid quartz vein type	

Abbreviations for inclusion description (at room temperature). a: CO_2-rich liquid with small CO_2 vapour; b: H_2O-rich liquid and CO_2-rich liquid; c: CO_2-rich liquid and H_2O-rich liquid ± small CO_2 vapour; d: H_2O-rich liquid and CO_2-hydrate with small CO_2 vapour; e: H_2O-rich liquid and CO_2 hydrate; (i): constant phase ratios indicating trapping from a homogeneous liquid; (ii): variable phase ratios indicating trapping from a heterogeneous liquid; $T_{h_{CO_2}}$ L-V: homogenisation temperature with CO_2 phase; $T_{m_{ice}}$: final melting of ice; $T_{m_{CO_2}}$: initial melting of CO_2 phase; T_{Clath}: final melting of clathrate; T_h: total homogenisation inclusion contents; wt% NaCl equiv.: salinity; d_{CO_2}: density of CO_2; d_{H_2O}: density of H_2O; d_{total}: total density; X_{CO_2}: mole fraction of CO_2; X_{NaCl}: mole fraction of NaCl.

A high salinity range in the base metal episode might indicate either separate stages of mineralisation or boiling in the mine portion close to the graphite zone (Fig. 2), or are due to fluid-rock interaction (Bottrell *et al.*, 1988). Meanwhile, the lower CO_2 densities (<0.70 g cm^{-3}) in some inclusions of the base metal episode may reflect a re-equilibrium of the fluid, possibly by either residual fluid inclusions of the pyrite episode or development during the late stage of the base metal episode formation.

The T_h of the fluid inclusions from the pyrite episode are homogenised at lower temperatures (265–295°C, clustered near 272°C) than those from the base metal episode (330–365°C, clustered near 342°C) (Table 2 and Fig. 4).

The transitional stage

The T_{Clath} of CO_2-rich inclusions in the quartz-carbonate phase ranges from 4.0 to 6.5°C (Fig. 5C). It is recognised as a jagged interface between the CO_2-vapour phase and the H_2O-liquid phase, when the crystals are coated with liquid CO_2. The $T_{m_{ice}}$ of the fluid inclusions from the quartz-carbonate phase exhibit a higher cluster centre (-6.0°C) than the barren quartz veins (-6.75°C) (Table 2 and Fig. 5D). These correspond to the maximum salinity estimated in the

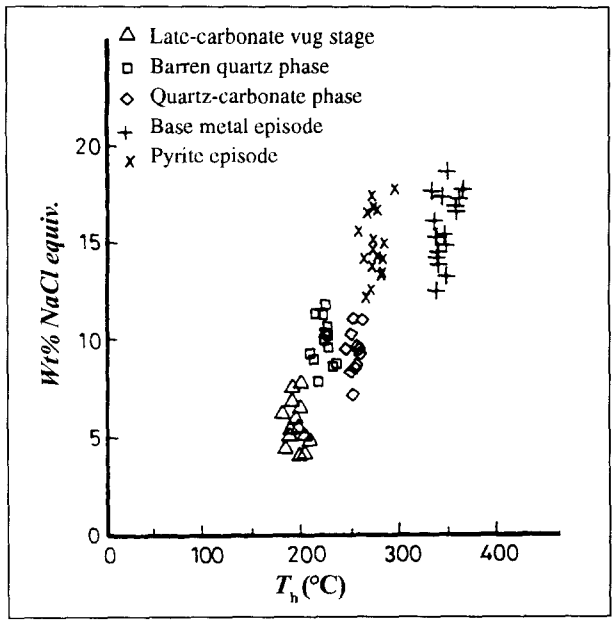

Figure 4. Plot of salinity (wt.% NaCl equiv.) versus final homogenisation temperature (T_h) in the El Sid Gold Mine area. Three continuum hydrothermal stages are distinguished.

quartz-carbonate phase, which range from 7 to 11 wt% equiv. (average 9.5 wt% equiv.) in aqueous phase. These values are relatively lower than that in the barren quartz veins (7–12 wt% equiv. average 10.5 wt% equiv.; Table 2 and Fig. 4).

The T_{mCO_2} of the quartz-carbonate phase (Table 2 and Fig. 5A) falls around -57.5 to -56.0°C with the centre near -56.8°C. The T_{hCO_2}L-V fall within the range 18.5–21.5°C clustering near 19.8°C (Fig. 5B). The estimated CO_2 densities of these fluid inclusions reveal a narrow range from 0.72 to 0.79 g cm^{-3}, and CO_2 concentrations range from 34 to 62 mole%. T_h measured in primary fluid inclusions in quartz from quartz-carbonate and barren quartz veins range from 245 to 265°C and from 210 to 235°C, respectively (Table 2 and Fig. 4).

The late carbonate vug stage

The T_{Clath} of the fluid inclusions in calcite from the late carbonate vug stage range between 4.5 and 7.5°C, clustering near 7.3°C (Fig. 5C). The detected T_{Clath} falls below and close to the quadruple point

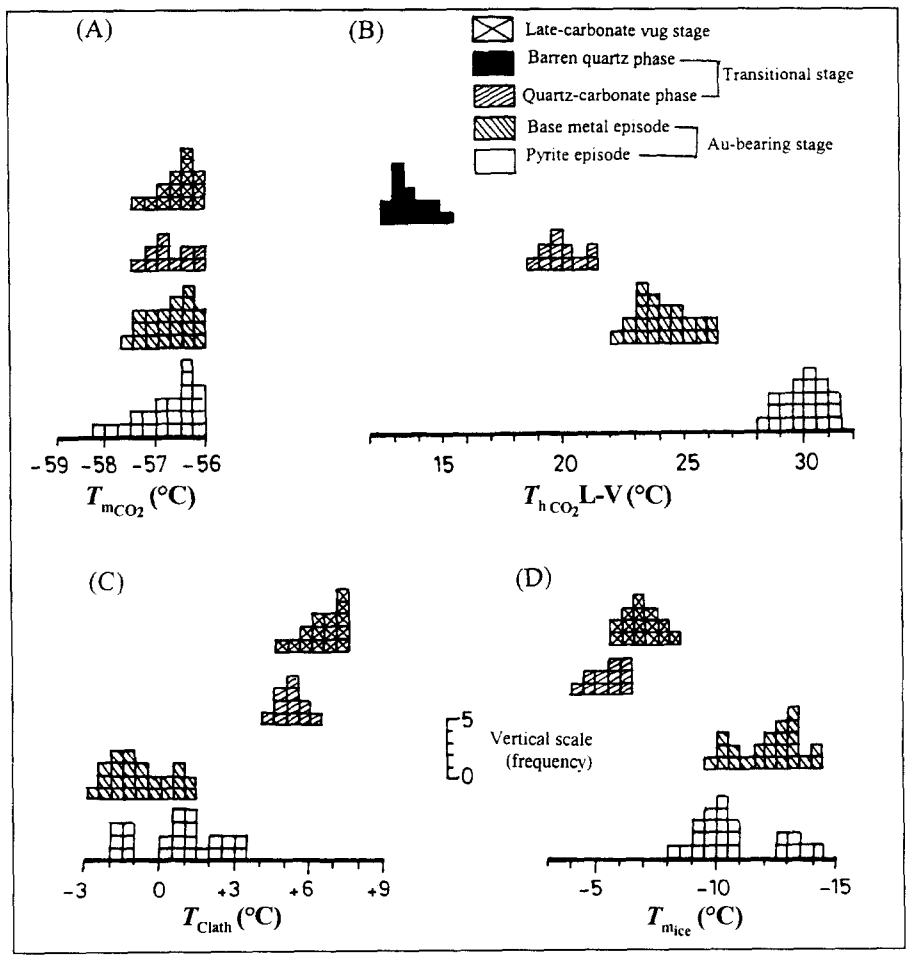

Figure 5. Histograms representing the microthermometric data of: (A) the initial melting temperature of the CO_2 phase (T_{mCO_2}); (B) the final homogenisation temperature of the CO_2-rich phases (T_{hCO_2}L-V) (Nb. Homogenisation to vapour phase); (C) the final clathrate temperature of decomposition of CO_2-hydrate (T_{Clath}); and (D) the final melting temperature of ice (T_m), in the different stages at El Sid Gold Mine.

(10°C) indicating the presence of minor amounts of salt (4–8 wt% equiv.; Fig. 4) and/or N_2 within the inclusions (Burruss, 1981). However, $T_{m_{CO_2}}$ (Fig. 5A) may indicate the presence of other volatile species associated with the late stage of the ore forming process. The freezing point depression is consistent with the presence of 28.8–51.6 mole% CO_2 within the aqueous phase. The $T_{h_{CO_2}}$L-V from the late carbonate vug stage show a wide range from 12.5 to 15.5°C, clustering near 13.3°C (Fig. 5B). The estimated CO_2 densities of these inclusions reveal a narrow range from 0.82 to 0.87 g cm^{-3} (Table 2), reflecting the presence of 28.8–51.6 mole% CO_2.

The T_h of the fluid inclusions in calcite from the late carbonate vug stage, which ranges from 180 to 210°C (Table 2 and Fig. 4), is relatively low compared with the other examined materials. This marked decrease in temperature and salinity may suggest that the fluids of the late carbonate vug stage had been cooled and diluted by meteoric water. This argument is further reinforced by O isotope data (see later).

Pressure considerations

The Au-bearing stage is characterised by fluid inclusions showing a wide range of CO_2:H_2O ratios, possibly due to unmixing of the original fluids through a pressure decrease (Wood *et al.*, 1986). The barren quartz phase of the transitional stage, as well as the calcite crystals of the latecarbonate vug stage, are characterised by two phase inclusions: a H_2O-rich liquid-vapour (barren quartz vein) and CO_2-rich inclusions (calcite crystals). Both display a similar homogenisation temperature and represent the waning stage of mineralisation. On boiling or near boiling, the fluids trapped in an inclusion fall on the liquid-vapour curve and, therefore, a further pressure correction is not necessary to estimate the confining pressure. However, the presence of CO_2 will shift the vapour pressure curves downward, if it occurs in a considerable amount (Takenouchi and Kennedy, 1964, 1965). Using the estimated fluid density and final T_h (Table 2), the confining pressures (figs 9–14 in Roedder, 1984) and depths (table 1b in Haas, 1971) of the different stages are found to be as follows:

i) Au-bearing stage:

a) pyrite episode: pressure (73–120 MPa) and depth (390–810 m).

b) base metal episode: pressure (115–170 MPa) and depth (1420–1800 m).

ii) Transitional stage:

a) Quartz-carbonate phase: pressure (89–115 MPa) and depth (390–560 m).

b) Barren quartz phase: pressure (18–31 MPa) and depth (175–325 m).

iii) Late carbonate vug stage: pressure (10–20 MPa) and depth (95–175 m).

The conditions of fluid entrapment during the Au-bearing stage at the El Sid Gold Mine could be estimated knowing the bulk composition of the parent fluid. Many inclusions from the El Sid Gold Mine contain ~28–62 mole% CO_2. Decrepitation of most of these inclusions of all sizes and prior to final homogenisation indicates a minimum trapping pressure of 100–200 MPa (Swanenberg, 1980). If it is assumed that these fluids were trapped on the solvus for the H_2O-CO_2 system containing 3–6 mole% NaCl with temperatures of 280–350°C, then the trapping should occur at pressures between 120–170 MPa (~800–1800 m depth), comparable to the values quoted above. The pressure estimates will be even greater if more volatile species are considered, such as CH_4 and N_2 (Hollister and Burruss, 1976).

STABLE ISOTOPES

Oxygen isotopes

Oxygen isotope data are shown in Table 3 and depicted in Figs 6 and 7. The measured $\delta^{18}O$ values of quartz samples fall between +10.6 and +14.5‰, while those in the calcite range from +9.3 to +16.3‰. Although most of the studied samples are in isotopic equilibrium ($\Delta^{18}O_{quartz\text{-}calcite}$ ranges from +1.0 to +1.4‰), the two samples, nos 48 and 49, from the pyrite episode are not in isotopic equilibrium (-1.8 and -1.9‰, respectively). Such inverted isotopic fractionation values (quartz/calcite), besides their relatively higher isotopic fractionation, might suggest that the quartz and calcite were formed at different times from different fluids or alternatively altered by isotopic exchange with meteoric/metamorphic waters.

The O isotope temperatures (Table 3) are calculated using the quartz-calcite fractionation equations of Matsuhisa *et al.* (1979) and O'Neil *et al.* (1969). The quartz-calcite isotopic temperatures of the Au-bearing stage show a wide range from 282 to 353°C. The pyrite and base metal episodes (Table 3) display isotopic temperatures ranging from 282 to 298°C and 334 to 353°C, respectively. These isotopic temperatures are consistent with the fluid inclusion T_h (Table 3). The temperature range of the base metal episode is comparable with many other mesothermal vein-type Au deposits (200–400°C: Groves and Foster, 1993; Nesbitt, 1993).

Using the final T_h (Table 3) to calculate $\delta^{18}O$ values of water in equilibrium with the quartz, the range of calculated $\delta^{18}O_{H_2O}$ values in the Au-bearing stage (Table 3) is +3.2 to +7.8%. The base metal episode displays higher $\delta^{18}O_{H_2O}$ values in equilibrium with the

Table 3. Measured and calculated O and H isotopic compositions of the quartz and calcite minerals in the El Sid Gold Mine, Eastern Desert, Egypt

Mineralisation stage	Sample no.	$\delta^{18}O$(%) Quartz	$\delta^{18}O$(%) Calcite	$\Delta^{18}O$ Qz-Cc	δD (%) Calcite	$\delta^{18}O_{H_2O}$	δD_{H_2O}	T^* (°C)	T_h^{**} (°C)
						Calculated			
Pyrite episode	LI, 5	11.10	9.80	1.30	-85	4.15	-55	298	290
Pyrite episode	LI, 9	10.69	9.30	1.39	-81	3.20	-59	283	280
Base metal episode	LI, 16	11.20	10.19	1.01	-78	5.98	-62	353	340
Base metal episode	LII, 24	12.50	11.40	1.10	-93	6.74	-47	334	350
Base metal episode	LII, 44	10.63	9.60	1.03	-105	5.29	-35	348	345
Base metal episode	LII, 47	12.60	11.50	1.10	-101	6.84	-39	334	315
Pyrite episode	LII, 48	13.60	15.50	-1.90	-62	6.70	-78	--	299
Pyrite episode	LII, 49	14.50	16.30	-1.80	-64	7.78	-76	--	304
Pyrite episode	LIII, 55	11.40	10.00	1.40	-87	3.86	-53	282	270

$\delta^{18}O$ values and δD values are expressed in ‰ derivation from SMOW. Abbreviations are as follows: Qz: quartz; Cc: calcite; T: temperature; LI: level one; LII: level two; LIII: level three.

*: Temperature based on co-existant quartz-calcite O isotope fractionations; $T°C_{quartz\text{-}calcite}$ were calclated from the following equations: ln $\alpha_{calcite\text{-}water} = 2.78(10^6T^{-2})$-2.89 (O'Neil *et al.*, 1969); ln $\alpha_{quartz\text{-}water} = 3.34(10^6T^{-2})$-3.31 (Matsuhisa *et al.*, 1979).

**T_h: Final homogenisation temperature of fluid inclusions in each sample. T_h was used to calculate $\delta^{18}O_{H_2O}$.

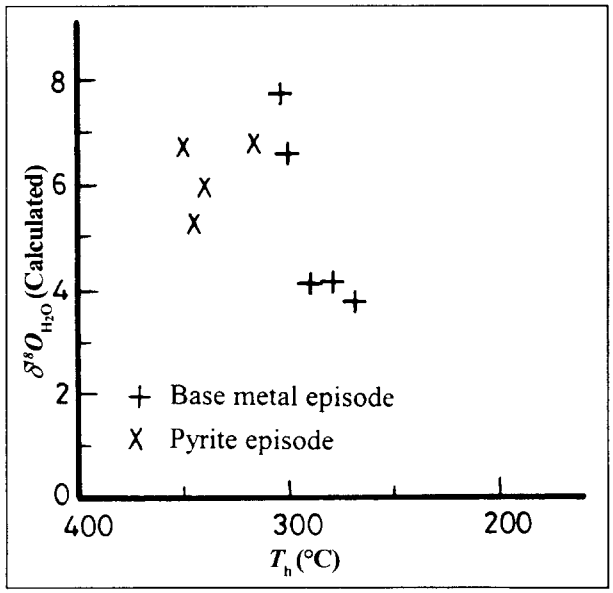

Figure 6. *Calculated O isotope compositions of water in equilibrium with quartz plotted against the corresponding final homogenisation temperatures (T_h).*

quartz (+5.3 to +6.8%) than the pyrite episode (+3.2 to +7.8%). However, sample nos 48 and 49 from the pyrite episode show the highest $\delta^{18}O$ values of water in equilibrium with the quartz among the analysed samples which might be attributed to mixing or water/rock interactions.

Hydrogen isotope data

The measured δD in calcite in the studied samples give much constructive information on the nature of the ore bearing fluids at the El Sid Gold Mine. In order to assess the importance of meteoric water in the El Sid Au hydrothermal system and interpret the calculated δD values of water in equilibrium with the calcite mineral, it is important to know the δD value of local meteoric water at the time of mineralisation (i.e. palæowater). This value has been estimated by two methods:

i) There is an apparent decrease in the calculated $\delta^{18}O_{H_2O}$ values of water with decreasing homogenisation temperatures from 400 to 200°C in the El Sid hydrothermal system (Fig. 6). Extrapolation of a least-squares regression line through these data (slope = 0.065, R = 0.80) has a $\delta^{18}O$ intercept of -18.7‰ at a temperatures of 15°C. This $\delta^{18}O$ value of -18.7‰ corresponds to meteoric water, which would have a δD value of -140‰ along the meteoric water line (Craig, 1961).

ii) The total range of measured δD values in calcite minerals is -105 to -62‰ (Table 3). More negative δD values may be expected during local meteoric waters exchange at the time of mineralisation.

Based on these two approaches, a δD value of approximately -140‰ has been assumed for the local meteoric water at El Sid at the time of mineralisation. Figure 7 shows the distribution of calculated water

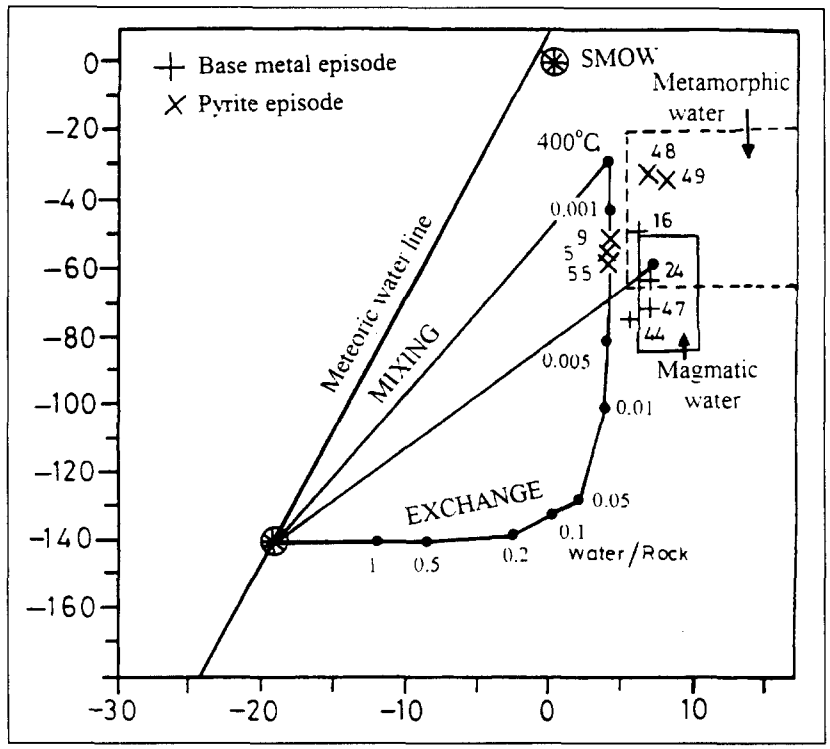

Figure 7. *Plot of calculated δD_{H_2O} versus $\delta^8O_{H_2O}$ for the Au-bearing stage at the El Sid Gold Mine. The mixing line shows values for hydrothermal mineral compositions which could result from mixing of a magmatic, metamorphic or highly exchanged meteoric waters with unexchanged meteoric water (δD_{H_2O}=-140‰). The pathway of the exchange curve shows hydrothermal mineral compositions which could result from isotopic exchange of a meteoric water with granitic rocks (δD = -70‰, δ^8O = +7‰) at 400°C and variable water/rock ratios (from Campbell* et al., *1984), calculated from the equations of Taylor (1974, 1978) and Ohmoto and Rye (1974).*

at the El Sid Gold Mine on a conventional H versus O isotope diagram. The δD values of the Au-bearing stage have a wide range (-75 to -32‰), indicating a magmatic and/or metamorphic signature on the ore-bearing fluid. The samples from the base metal episode show relatively lower δD values (-75 to -48‰) than those of the pyrite one (-57 to -32‰). The isotopic data from the base metal episode fall within the calculated range of magmatic water (Taylor, 1979) and may therefore represent primary magmatic water or at least some water from any source whose isotopic composition is controlled by exchange with the Fawakhir granitoid rocks at magmatic temperatures. Most of samples from the pyrite episode have values outside the range of magmatic or metamorphic waters toward the lower $\delta^{18}O$ values, but sample nos 48 and 49 from the pyrite episode fall within the range of metamorphic water (Taylor, *op. cit.*). These values could be attributed to progressive mixing of mag-matic water with meteoric water (Fig. 7) or exchange of local meteoric water with granite or serpentinite rocks at elevated temperatures and low water/rock ratios. A 400°C exchange curve (after Campbell *et al.*, 1984) shown in Fig. 7 suggests water/rock ratios between 0.001 and 0.005 during the early times of Au deposition. Using either a mixing or exchange model, it is evident that the isotopic compositions of the El Sid Au mineralisation were largely controlled by the host granitic and serpentinitic rocks.

The data of the δD and $\delta^{18}O$ values at the El Sid Gold Mine are consistent with other well-known mesothermal Au deposits, (e.g. Canadian Cordilleran Au deposits, Archæan Au deposit of Australia: Nesbitt and Muehlenbachs, 1989). Comparison of these data with other Egyptian localities is not possible due to the lack of available published data.

DISCUSSION

The vein-type Au deposits in eastern Egypt are, generally characterised by polymetallic sulphide assemblage, formed at shallow depths under mesothermal conditions (Garson and Shalaby, 1976). The source of the ore-bearing fluids are related either to a fluid phase of the Gattarian Granite, Lower Palæozoic age (Hussein, 1990) or to Late Precambrian subduction-related calc-alkaline magmatism (El-Gaby *et al.*, 1988). The mineralised solution were induced

either by metamorphism or cooling (Pohl, 1988). Leaching and remobilisation from a hidden source are advocated by Harraz and El-Dahhar (1993). To assess the origin and nature of the mineralising fluids, as well as the appropriate genetic model which could explain the geologic setting, mineralogical, microthermal and isotopic characters at the El Sid Gold Mine, it becomes relevant to address the nature and origin of ore fluids.

Nature and origin of ore fluids

A part of the Au-bearing stage, the pyrite episode, has $T_{h_{CO_2}}$ L-V (28.0–31.5°C) markedly higher than the base metal one (22.0–26.5°C). This anomalous behaviour is attributed to the presence of an extra gas and/or salt phase. In addition, many of T_{Clath} of both episodes were below 10°C, indicating minor amounts of salt within the inclusions. Moreover, the $T_{m_{CO_2}}$ measurements reveal that the deposition of the Au is largely affected by wall rock interaction as manifested by the inferred occurrence of CH_4 phase in some samples collected from the graphite materials along serpentinite-granite contact.

Previous studies on the fluid inclusion of the Au deposits limit the fluid source to three possibilities:

i) a meteoric/volcanic(?) source such as that of epithermal Au deposits;

ii) a hypabyssal magmatic source; and

iii) a metamorphic source.

According to the geological setting of the El Sid mineralised quartz veins, the following may be concluded:

i) The large quartz veins are epigenetically formed in a subduction zone, from a direct magmatic fluid.

ii) The quartz veins invaded the granitic pluton and occasionally extend into the adjacent serpentinite-talc carbonate rocks through a thick zone of graphite materials.

iii) The Au-bearing quartz veins are structurally controlled by the younger strike-slip faulting systems (north-northeast and east-northeast) that formed during the Pan-African tectonic event and affected the northern part of the Eastern Desert (El-Gaby *et al.*, 1988).

During this deformational event, faulting seems to have resulted in hydraulic fracturing. The hydraulic fractures acted as favourable sites of localising the Au deposit at northern and western contacts of Fawakhir granitoid pluton with serpentinite rock. Moreover, the microthermometric investigation emphasises that there were multiple mineralisation events. The increase of salinity from 12 to 19 wt% equiv. and T_h from 265 to 365°C of the H_2O-CO_2-rich studied fluid inclusions, do not support a direct magmatic source of the ore fluids. It is more likely that the ore-bearing fluids were mixed by fluids of metamorphic origin and attained their metal contents from the participation of a geothermal convective system, during the water/rock interactions.

The characters of the El Sid Au deposits resemble those of the Archæan Au deposit; all imply mesothermal conditions between 250–350°C at 150–300 MPa (Colvine, 1989; Groves and Foster, 1993). Like most of the Archæan Au deposits, the El Sid Au deposit exhibits a pinch and swell vein texture and evidence of multiple mineralisation events (Sibson *et al.*, 1988). The preferred model for the formation of the El Sid Au deposit is under brittle ductile and brittle transition shear zone of deformation in the earth's crust linked to hydrothermal fluid valving along the vein failure surface (Sibson, 1990). However, the estimated salinity from the studied fluid inclusions are not low as in the Archæan mesothermal Au deposits. These fluid inclusion characters cannot unequivocally define one single fluid source, but are compatible with magmatic/metamorphic sources, later modified by reaction with the wall rock during the mineralising event (Marmont, 1983). To clarify the source of H_2O-CO_2-rich fluids, the stable isotope study indicates a role for exchange between meteoric and magmatic-metamorphic waters (Fig. 7). So, the source of H_2O-CO_2-rich fluids could be the Fawakhir granitoid pluton, mixed with fluids existing at quite shallow crustal levels (Garrels and Richter, 1955) creating hydrothermal convection systems. Such a hypothesis of fluid pressure drops postdating fracture failure at the end of the pyrite episode has great implications, which could contribute to the origin and source of the ore-bearing fluids. A drop in fluid pressure is likely to induce fluid immiscibility in a complex H_2O-CO_2-NaCl fluid (Spooner *et al.*, 1987), which further aids precipitation of the vein minerals (Drummond and Ohmoto, 1985).

Transport and deposition of Au

The presence of sulphide minerals among the other silicate phases in the granite host indicate the role of liquid immiscibility during the crystallisation history of the magmatic liquid (Drummond and Ohmoto, 1985) as the granitic magma approached S saturation level. In this model, Au is originally present in the magmatic liquid and, because of its chalcophile affinity, it will be admitted into the sulphide minerals (Keays, 1984); otherwise, it will be dispersed throughout the magma. Thus, the formation of sulphides would play a significant role for concen-trating Au, which later could be leached and mobilised during reduction, fracturing and alteration of the Au-bearing sulphide. During the alteration of the serpentinite rocks to talc-carbonate and graphite materials, water was produced from the breakdown of the ferromagnesian minerals

in addition to water expelled from the magma itself. In the El Sid Gold Mine area, the heat source necessary to drive the convective system might have been attributed to the cooling Fawakhir granitoid pluton. The driving force for circulating water in the convection cells throughout the fractured zones caused leaching, transportation and concentration of Au. The Au is most likely transported as a bisulphide complex, since the Au was associated with H_2O-CO_2-rich fluids having an alkaline to near neutral character (Seward, 1993). Precipitation of Au in the El Sid Gold Mine may be attributed to decreasing ligand activity involving the formation of Fe sulphides from wall rock Fe oxides and silicates (Seward, 1973, 1993). In the Fawakhir granitoid rocks, the mineral association may be explained by the partitions of HS^- into the non-aqueous phase during fluid immiscibility (Spooner *et al.*, 1987).

Fluid inclusion studies of Au mineralisation indicate that in ore fluid containing CO_2-rich and H_2O-rich phases, the immiscibility between CO_2 and H_2O plays an integral part in Au deposition in mesothermal vein systems (Goldfarb *et al.*, 1989). In the light of the experimental system H_2O-CO_2-NaCl (Bowers and Helgeson, 1983), the data of the present study indicates that the two volatile species will remain unmixed at 150 MPa, temperatures above 265°C and salinities 3–6 mole% NaCl when the CO_2 exceeds 15 mole% (Naden and Shepherd, 1989). Because of the relatively high solubility of CO_2 at elevated temperatures (280–350°C) and pressures (120–150 MPa), the extent of reaction needs much greater immiscibility in the El Sid Au deposit. Thus, in the *P-T* range under consideration, fluid immiscibility and precipitation of Au is favoured by wall rock interactions with graphite materials that produce a small amount of methane (that is, under reducing conditions where the ambient f_{O_2} is low). Close to the graphite materials in the central part of the El Sid Gold Mine, the addition of small amounts of methane which enlarges the *P-T* field of immiscibility and acts as a powerful trigger for Au deposition is expected (Sibson *et al.*, 1988). The formations of the graphitic materials may be attributed to emplacement of the Fawakhir granitoid into the serpentinite-talc-carbonate rocks through the reduction of talc-carbonate materials.

The conditions of deposition at the El Sid Au deposit are comparable with many other mesothermal vein systems quoted in the literature (Nesbitt and Muehlenbachs, 1989; Groves and Foster, 1993; Nesbitt, 1993). The loss of CO_2 and other volatiles from the fluid phase during boiling will cause an increase of the pH, lower the f_{O_2}, and decrease the temperature and activity of the bisulphide complex (Drummond and Ohmoto, 1985; Seward, 1993). At the same time, total S is decreasing due to volatilisation of H_2S and precipitation of sulphides. The reducing process of the total S has an ultimate effect of approaching the Au super saturation and precipitation. These would effectively destablise the Au bisulphide complex and lead to deposition of Au as well as the silicate and carbonate gangue.

CONCLUSIONS

The El Sid Au deposit formed in at least two successive episodes. The early one started with the formation of a coarse-grained pyrite with arsenopyrite from mineralised solution having H_2O-CO_2-rich fluids(29–57 mole% CO_2 and densities 0.51–0.66 g cm^{-3}), moderate salinity (14.5 wt% equiv.) and final T_h of about 272°C. The later episode started after a distinct time interval with the fracturing of the Au-bearing quartz veins, and is characterised by the assemblage of streaky pyrite-sphalerite-galena. The latter was formed from mineralising solutions characterised by H_2O-CO_2-rich fluids (<62 mole% CO_2), low CO_2 density (<0.70 g cm^{-3}), high salinity (17.5 wt% equiv.) and final T_h of about 343°C. It is evident that exchange between the ore-bearing fluids of the pyrite episode and metamorphic water, imparted a slight change in composition and re-equilibration of the fluid inclusions of the first episode.

Gold deposition occurred at temperatures above 280°C and at pressures at least 120 MPa (>1800 m in depth) and largely related to fluid wall rock interaction. Gold was repeatedly deposited during these two major episodes, being more enriched in the early part of the base metal episode. This may explain why the Au is mainly detected as infiltrations along microfractures of pyrite and arsenopyrite crystals and as irregular blebs in the sphalerite. The presence of brecciation and precipitation of carbonate and graphitic materials indicated that:

i) immiscibility processes have taken place during Au formation; and

ii) the Au precipitation was accomplished through reduction by carbon according to the equations:

$$C + 2H_2O \rightarrow CO_2 + 2H_2; \text{ and}$$
$$4Au(HS)_2^- + 8H^+ \rightarrow 4Au^\circ + 8H_2S$$

Dissolution and transportation of the Au might have been achieved through complexing as a bisulphide complex, which is comparable with several mesothermal Au occurrences all over the world. Precipitation of Au in the El Sid Gold Mine may be attributed to decreasing ligand activity involving the formation of Fe sulphides from wall rock Fe oxides and silicates. Meanwhile, the late phases of mineralisation can be related to progressive dilution by the meteoric water.

ACKNOWLEDGEMENTS

The author is grateful to Prof. El-Dahhar, Geology Department, Alexandria University for reading the manuscript. The assistance of Dr Tom Anderson, Geologic Museum, Oslo University, Norway during the fluid inclusion analyses is deeply acknowledged. *Editorial handling - G.J.H. Oliver & S. Bottrell*

REFERENCES

Bottrell, S.H., Shepherd, J.J., Yardley, B.W.D., Dubessy, J., 1988. A fluid inclusion model for the genesis of the ores of the Dolgellau Gold Belt, North Wales. Journal Geological Society London 145, 139–145.

Bowers, T.S., Helgeson, H.C., 1983. Calculation of the thermodynamic and geochemical consequences of nonideal mixing in the system H_2O-CO_2-NaCl on phase relations in geologic systems: Metamorphic equilibria at high pressures and temperatures. American Mineralogist 68, 1059–1075.

Burruss, R.C., 1981. Analysis of phase equilibria in C-O-H-S fluid inclusions. In: Hollister, L.S., Crawford, M.L. (Eds.), Short Course in Fluid Inclusions. Applications to Petrology. Mineralogical Association Canada Short Course Handbook 6, pp. 39–74.

Campbell, A., Rye, D., Petersen, U., 1984. A hydrogen and oxygen isotope study of the San Cristobal mine, Peru: Implications of the role of water to rock ratio for the genesis of wolframite deposits. Economic Geology 79, 1818–1832.

Collins, P.L.F., 1979. Gas hydrates in CO_2-bearing fluid inclusions and the use of freezing data for estimation of salinity. Economic Geology 74, 1435–1444.

Colvine, A.C., 1989. An empirical model for the formation of Archæan gold deposits: products of final cratonization of the Superior Province, Canada. In: Keays, R.R., Ramsay, W.R., Groves, D.I. (Eds.), The Geology of Gold Deposits: The Perspective in 1988. Economic Geology Monograph 6, pp. 37–53.

Craig, H., 1961. Isotopic variations in meteoric waters. Science 133, 1702–1703.

Drummond, S.E., Ohmoto, H., 1985. Chemical evolution and mineral deposition in boiling hydrothermal systems. Economic Geology 80, 126–147.

El-Bouseily, A.M., El-Dahhar, M.A., Arslan, A.I., 1985. Ore-microscopic and geochemical characteristics of gold bearing sulfide minerals, El Sid Gold Mine, Eastern Desert, Egypt. Mineralium Deposita 20, 194–200.

El-Dahhar, M.A., 1995. Mineralogic and wallrock alteration studies in and around gold-bearing quartz veins at El Sid Gold Mine area, Eastern Desert, Egypt. Bulletin Faculty Science, Alexandria University 35, 151–168.

El-Gaby, S., List, F.K., Tehrani, R., 1988. Geology, evolution and metallogenesis of the Pan-African Belt in Egypt. In: El-Gaby, S., Greiling, R.O. (Eds.), The Pan-African Belt of Northeast Africa and Adjacent Areas. Friedrich Vieweg und Sohn, Braunschweig, Wiesbaden, pp.17–68.

El-Mezayen, A.M.A., 1983. Geology and petrology of the basement rocks in the Fawakhir area, central Eastern Desert, Egypt 'El Fawakhir ophiolites'. Ph.D. thesis, Al Azhar University, Egypt, 248p.

Garrels, R.M., Richter, D.M., 1955. Is carbon dioxide an ore-forming fluid under shallow earth conditions? Economic Geology 50, 447–457.

Garson, M.S., Shalaby, I., 1976. Precambrian-lower Palæozoic plate tectonics and metallogenesis in the Red Sea region. Geologic Association Canada, Special Paper 14, 573–596.

Goldfarb, R.J., Leach, D.L., Rose, S.C., Landis, G.P., 1989. Fluid inclusion geochemistry of gold-bearing quartz veins of the Juneau Gold Belt, Southeastern Alaska: Implications for ore genesis. In: Keays, R.R., Ramsay, W.R., Groves, D.I. (Eds.), The Geology of Gold Deposits: The Perspective in 1988. Economic Geology Monograph 6, pp. 363–375.

Groves, D.I., Foster, R.P., 1993. Archæan lode gold deposits. In: Foster, R.P. (Ed.), Gold Metallogeny and Exploration. Chapman and Hall, London, pp. 63–103.

Haas, J.L., Jr, 1971. The effect of salinity on the maximum thermal gradient of a hydrothermal system at hydrostatic pressure. Economic Geology 66, 940–946.

Harraz, H.Z., 1985. Geochemical prospecting for gold in some localities in the Eastern Desert of Egypt. M.Sc. thesis, Tanta University, Egypt, 281p.

Harraz, H.Z., Ashmawy, M.H., 1994. Structural and lithogeochemica constraints on the localization of gold deposits at the El Sid-Fawakhir Gold Mine area, Eastern Desert, Egypt. Egyptian Journal Geology 38, 629–648.

Harraz, H.Z., El-Dahhar, M.A., 1993. Nature and composition of gold-forming fluids at Umm Rus area, Eastern Desert, Egypt: evidence from fluid inclusions in vein materials. Journal African Earth Sciences 16, 341–353.

Ho, S.E., Groves, D.I., Phillips, G.N., 1985. Fluid inclusions as indicators of the nature and source of ore fluids and ore depositional conditions for Archæan gold deposits of the Yilgarn Lock, Western Australia. Transactions Geological Society South Africa 88, 149–158.

Hollister, L.S., Burruss, R.C., 1976. Phase equilibria in fluid inclusions from the Khtada Lake metamorphic complex. Geochimica Cosmochimica Acta 40, 163–175.

Hussein, A.A.A., 1990. Mineral deposits. In: Said, R. (Ed.), The Geology of Egypt. A.A. Balkema, Rotterdam, pp. 511–566.

Keays, R.R., 1984. Archæan gold deposits and their source rocks: The upper mantle connection. In: Foster, R.P. (Ed.), Gold '82. Geologic Society Zimbabwe, Special Publication, A.A. Balkema, Rotterdam, pp. 17–52.

Marmont, S., 1983. The role of felsic intrusions in gold mineralization. In: Colvine, A.C. (Ed.), The Geology of Gold in Ontario. Ontario Geologic Survey, Miscellaneous Paper 110, pp. 38–47.

Matsuhisa, Y., Goldsmith, J.R., Clayton, R.N., 1979. Oxygen isotopic fractionation in the system quartz-albite-anorthite-water. Geochimica Cosmochimica Acta 43, 1131–1140.

Meneisy, M.Y., Lenz, H., 1982. Isotopic ages of some Egyptian granites. Annals Geological Survey Egypt 12, 7–14.

Naden, J., Shepherd, T.J., 1989. Role of methane and carbon dioxide in gold deposition. Nature 342, 793–795.

Nesbitt, B.E., 1993. Phanerozoic gold deposits in tectonically active continental margins. In: Foster, R.P. (Ed.), Gold Metallogeny and Exploration. Chapman and Hall, London, pp. 105–132.

Nesbitt, B.E., Muehlenbachs, K., 1989. Geology, geochemistry and genesis of mesothermal lode gold deposits of the Canadian Cordillera: Evidence for ore formation from evolved meteoric water. In: Keays, R.R., Ramsay, W.R., Groves, D.I. (Eds.), The Geology of Gold Deposits: The Perspective in 1988. Economic Geology Monograph 6, pp. 553–563.

Ohmoto, H., Rye, R.O., 1974. Hydrogen and oxygen isotopic compositions of fluid inclusions in the Kuroko deposits, Japan. Economic Geology 69, 947–953.

O'Neil, J.R., Clayton, R.N., Mayeda, T.K., 1969. Oxygen isotope fractionation in divalent metal carbonate. Journal Chemical Physics 51, 5547–5558.

Pohl, W., 1988. Precambrian metallogeny of Northeast-Africa. In: El-Gaby, S., Greiling, R.O. (Eds.), The Pan-African Belt of Northeast Africa and Adjacent Areas. Friedrich Vieweg und Sohn, Braunschweig, Wiesbaden, pp. 319–341.

Roedder, E., 1963. Studies of fluid inclusions II: freezing data and their interpretation. Economic Geology 58, 167–211.

Roedder, E., 1967. Fluid inclusions as samples of ore fluids. In: Barnes, H.L. (Ed.), Geochemistry of Hydrothermal Ore Deposits. 1st edition. Holt, Rhinehart, and Winston, New York, pp. 515–574.

Roedder, E., 1984. Fluid inclusions. Reviews Mineralogy 12, 1–644.

Rye, R.O., Sawkins, F.J., 1974. Fluid inclusion and stable isotope studies on the Casapalca Ag-Pb-Zn-Cu deposit, Central Andes, Peru. Economic Geology 69, 181–205.

Sabet, A.H., Bondonosov, V.P., 1984. The gold ore formations in the Eastern Desert of Egypt. Annals Geological Survey Egypt 14, 35–42.

Seward, T.M., 1973. Thio-complexes of gold in hydrothermal ore solutions. Geochimica Cosmochimica Acta 37, 379–399.

Seward, T.M., 1993. The hydrothermal geochemistry of gold. In: Foster, R.P. (Ed.), Gold Metallogeny and Exploration. Chapman and Hall, London, pp. 37–61.

Shepherd, T.J., 1981. Temperature-programmable, heating-freezing stage for microthermometric analysis of fluid inclusions. Economic Geology 75, 1244–1247.

Sibson, R.H., 1990. Faulting and fluid flow. In: Nesbitt, D.E. (Ed.), Fluids in Tectonically Active Regimes of the Continental Crust. Mineralogical Association Canada Short Course Handbook 18, pp. 91–132.

Sibson, R.H., Robert, F., Poulsen, K.H., 1988. High angle reverse faults, fluid pressure cycling and mesothermal gold deposits. Geology 16, 551–555.

Spooner, E.T.C., Bray, C.J., Wood, P.C., Burrows, D.R., Callan, N.J., 1987. Au-quartz vein and Cu-Au-Ag-Mo-anhydrite mineralization, Hollinger-McIntyre mine, Timmins, Ontario: $\delta^{13}C$ values (McIntyre), fluid inclusion gas geochemistry, pressure (depth) estimation, and H_2O-CO_2 phase separation as a precipitation and dilation mechanism. Ontario Geologic Survey Miscellaneous Paper 136, 35–56.

Swanenberg, H.E.C., 1980. Fluid inclusions in high-grade metamorphic rocks from southeast Norway. University Utrecht, Geologic Ultraiectina 25, 147p.

Takenouchi, S., Kennedy, G.C., 1964. The binary system H_2O-CO_2 at high temperatures and pressures. American Journal Science 262, 1055–1074.

Takenouchi, S., Kennedy, G.C., 1965. The solubility of carbon dioxide in NaCl solutions at high temperatures and pressures. American Journal Science 263, 445–454.

Taylor, H.P. Jr, 1974. The application of oxygen and hydrogen isotope studies to problems of hydrothermal alteration and ore deposition. Economic Geology 69, 843–883.

Taylor, H.P. Jr, 1978. Oxygen and hydrogen isotope studies of plutonic granitic rocks. Earth Planetary Science Letters 38, 177–210.

Taylor, H.P. Jr, 1979. Oxygen and hydrogen isotope relationships in hydrothermal mineral deposits. In: Barnes, H. H. (Ed.), Geochemistry of Hydrothermal Ore Deposits. Wiley, New York, pp. 236–277.

Wood, P.C., Burrows, D.R., Thomas, A.V., Spooner, E.T.C., 1986. The Hollinger-McIntyre Au-quartz vein system, Timmins, Ontario, Canada: geologic characteristics, fluid properties and light stable isotopes. In: Macdonald, A.J. (Ed.), Gold '86. Konsult International Inc, Willowdalda, Ontario, pp. 56–80.